PCCP

PAPER

View Article Online
View Journal | View Issue

Cite this: *Phys. Chem. Chem. Phys.*, 2016, **18**, 5720

Evolution of magnetization due to asymmetric dimerization: theoretical considerations and application to aberrant oligomers formed by apoSOD1^{2SH}

Ashok Sekhar,*[a] Alex D. Bain,[b] Jessica A. O. Rumfeldt,[c] Elizabeth M. Meiering[c] and Lewis E. Kay*[ad]

Received 26th May 2015,
Accepted 1st July 2015

DOI: 10.1039/c5cp03044g

www.rsc.org/pccp

A set of coupled differential equations is presented describing the evolution of magnetization due to an exchange reaction whereby a pair of identical monomers form an asymmetric dimer. In their most general form the equations describe a three-site exchange process that reduces to two-site exchange under certain limiting conditions that are discussed. An application to the study of sparsely populated, transiently formed sets of aberrant dimers, symmetric and asymmetric, of superoxide dismutase is presented. Fits of concentration dependent CPMG relaxation dispersion profiles provide measures of the dimer dissociation constants and both on- and off-rates. Dissociation constants on the order of 70 mM are extracted from fits of the data, with dimeric populations of ~2% and lifetimes of ~6 and ~2 ms for the symmetric and asymmetric complexes, respectively. This work emphasizes the important role that NMR relaxation experiments can play in characterizing very weak molecular complexes that remain invisible to most biophysical approaches.

Introduction

Both protein function and misfunction are often related to dynamics.[1,2] For example, binding of ligands to occluded sites in proteins can only occur through molecular rearrangements that provide a pathway or pathways for entry.[3] Enzymatic activity can be predicated on lid movement or the correct juxtaposition of catalytic residues that sometimes only occurs transiently *via* motion[4–6] and abnormal enzyme conformational dynamics can be linked to disease.[7] Molecular recognition can proceed *via* conformational selection, induced fit or some combination of these processes that also requires plasticity of the interacting partners.[8,9] Dynamic loop regions in proteins can play important roles in the transmission of allosteric signals[10] and more generally it is becoming increasingly recognized that intrinsically disordered proteins, that are highly dynamic, play important roles in a wide range of functions in the cell.[11] The relation between dynamics and misfunction has been strengthened with the realization that aberrant protein conformations can be generated through conformational fluctuations from the ground state that expose aggregation prone regions of structure.[12,13] Locally unfolded states have been implicated as key precursors in the aggregation of a number of proteins involved in human disease[12] such as transthyretin (TTR),[14–16] human lysozyme,[17] superoxide dismutase[12,18–21] and β2-microglobulin.[22]

Although generating static three-dimensional pictures of protein molecules is an important first step in understanding function, it is now clear that insight into how structure changes with time, over a broad range of time-scales, is also critical. Solution NMR spectroscopy is a powerful technique for studies of protein dynamics and over the past many years a large number of experiments have been proposed for sampling different time-scales of motion at many sites in the molecule of interest.[23–27] Studies of conformational dynamics occurring on the millisecond timescale, using experimental approaches originally conceived many decades ago,[28–30] have recently enjoyed a resurgence.[26,31] In one class of experiment, termed Carr–Purcell–Meiboom–Gill (CPMG) relaxation dispersion, the effective transverse relaxation rates of probe spins are modulated as a function of the number of refocusing pulses applied during an interval of fixed duration.[24,32] In a second method, Chemical Exchange Saturation Transfer (CEST),[30] the effect of a radio-frequency perturbation applied at the resonance position of a spin in the minor state conformation

[a] *Departments of Molecular Genetics, Biochemistry and Chemistry, The University of Toronto, Toronto, Ontario, M5S 1A8, Canada. E-mail: ashok.sekhar@utoronto.ca, kay@pound.med.utoronto.ca*
[b] *Department of Chemistry and Chemical Biology, McMaster University, Hamilton, Ontario, L8S 4M1, Canada*
[c] *Department of Chemistry, University of Waterloo, 200 University Avenue West, Waterloo, Ontario, N2L 3G1, Canada*
[d] *Hospital for Sick Children, Program in Molecular Structure and Function, 555 University Avenue, Toronto, M5G 1X8, Ontario, Canada*

is transferred to the major state correlation for detection.[25,33] The utility of both of these experiments is made clear by the fact that it is possible to extract site-specific chemical information on sparsely populated and transiently formed conformers that are otherwise 'invisible' to traditional NMR experiments and in most cases to standard biophysical methods as well.[26] Analysis of the resulting CPMG or CEST profiles using the appropriate model of chemical exchange leads to the extraction of kinetic and thermodynamic parameters of the exchange event(s) as well as chemical shift differences between probes in each of the exchanging states. An advantage of CEST is that so long as the shift differences between corresponding nuclei in each of the exchanging states are sufficiently large, so that major and minor state peaks are resolved, it is possible to obtain resonance positions in the excited state by inspection; however extraction of additional information is still predicated on fits of the data.[33]

The majority of CPMG or CEST relaxation data are fit to a simple model of two-site chemical exchange. A number of different models of exchange have also been considered in addition to the simple two-site A ↔ B exchange process, including protein–ligand binding as well as formation of a symmetric *n*-mer complex from *n* protomers.[24] Herein, we derive a set of coupled equations describing magnetization exchange for a reaction scheme in which a pair of equivalent monomers form an asymmetric dimeric complex, a situation which to the best of our knowledge has not been considered before. We show that expressions can be derived in a straightforward manner by considering in parallel a set of kinetic equations that pertains to each of the spin states (spin α/β for a spin 1/2 system) of the exchanging spin. An application to the study of conformational exchange in superoxide dismutase (SOD1) is presented.

Results and discussion

Motivation of the problem

SOD1 is an antioxidant enzyme that has been extensively studied as a model system for how protein misfolding relates to neurodegenerative disease.[34] Misfolded conformers of SOD1 have been hypothesized to be the toxic disease causing species in amyotrophic lateral sclerosis[35] with SOD1 aggregates found in neuronal cells of patients.[36,37] Although the dimeric, Cu-, Zn-metal bound and disulfide form of the protein is very stable and highly soluble,[20,21,38,39] an immature form that lacks metal and the stabilizing intra-molecular disulfide (apoSOD1^{2SH}) has a much higher likelihood of misfolding and aggregating *in vitro*[21,39,40] and may be the primary cause of toxicity *in vivo*.[35] We have recently applied CEST and CPMG relaxation methods to study the conformational dynamics of this immature protein.[41] Notably, apoSOD1^{2SH} is extremely dynamic, with at least four separate conformational transitions that could be detected. Of these, two that are involved in the formation of non-native oligomers are of particular interest in what we describe here (referred to as processes III and IV, following the nomenclature in Sekhar *et al.*[41]). For these, analysis of ^{15}N and methyl

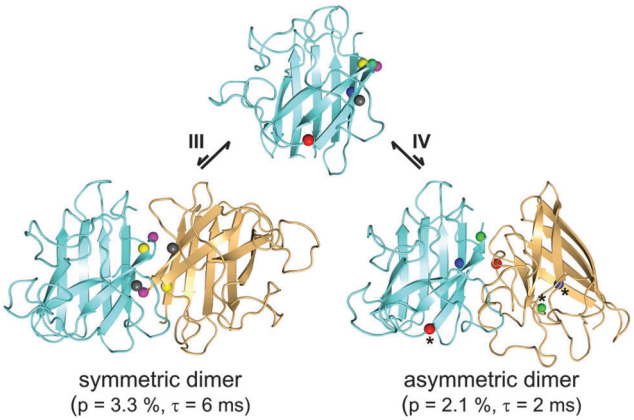

Fig. 1 Schematic illustrating exchange between ground state monomeric apoSOD1^{2SH} and symmetric (left) and asymmetric (right) excited state non-native dimers. Lifetimes (τ) and populations (*p*; total protein concentration of 1.3 mM) obtained by fitting CPMG relaxation data to the appropriate model of chemical exchange (see text) are indicated. A number of residues are highlighted in the monomer and in both dimeric structures that are involved in the different dimerization events (colors distinguish different sites, as well as probes of the two different dimerization processes). It is clear that in the asymmetric dimer one of the residues of the pair in each case (indicated with an asterisk) is in a similar environment as that in the monomeric ground state structure.

^{13}C relaxation dispersion data establishes that each process has a different temperature dependence and distinct kinetic and thermodynamic parameters. Both processes are concentration dependent with larger dispersion profiles obtained as the concentration of protein is increased that is consistent with protein oligomerization. The chemical shifts of excited states that were extracted from the CPMG data were subsequently used in a HADDOCK protocol[42] to generate the structures shown in Fig. 1, with symmetric (left, process III, non-native dimer (1)) and asymmetric (right, process IV, non-native dimer (2)) dimers obtained for the two processes. These structures are distinct from that of the symmetric native dimer associated with the mature, metal bound form of the enzyme. The fact that the shift restraints could only be fit by assuming that non-native dimer 2 is asymmetric led us to derive a set of equations describing magnetization exchange in the case of an asymmetric exchange event involving a pair of equivalent monomers. The resulting equations were then used to obtain accurate thermodynamic and kinetic parameters of the exchange process. In what follows we first present the derivation and subsequently consider the exchanging system illustrated in Fig. 1.

Derivation of magnetization exchange equations

We consider the exchange reaction,

$$2\mathrm{A} \underset{k_{-1}}{\overset{k_1}{\rightleftharpoons}} \mathrm{BC}, \qquad (1)$$

involving the dimerization of molecule A to form the product BC, focusing on a single spin throughout. We denote the product as BC and not A_2 to reflect the fact that while B and C are chemically equivalent to A (same protein in the application

considered below) the spin in question may not be in magnetically equivalent environments in each molecule so that different chemical shifts of the probe can, in principle, be obtained for A (ω_A), B (ω_B) and C (ω_C). We further focus initially on the exchange of Z-magnetization, although as we show below the results are equivalent for transverse magnetization components so long as additional terms for chemical shift evolution are included. For a spin 1/2 probe there are two eigenstates of the Zeeman Hamiltonian denoted by α and β. Thus we can 'expand' eqn (1) in terms of the eigenstates as

$$A_\alpha + A_\alpha \underset{k_{-1}}{\overset{k_1}{\rightleftharpoons}} B_\alpha C_\alpha \tag{2.1}$$

$$A_\alpha + A_\beta \underset{k_{-1}}{\overset{k_1}{\rightleftharpoons}} B_\alpha C_\beta \tag{2.2}$$

$$A_\beta + A_\alpha \underset{k_{-1}}{\overset{k_1}{\rightleftharpoons}} B_\beta C_\alpha \tag{2.3}$$

$$A_\beta + A_\beta \underset{k_{-1}}{\overset{k_1}{\rightleftharpoons}} B_\beta C_\beta \tag{2.4}$$

where subscripts α and β denote the spin-state of the probe spin in question. The microscopic rate constants for each of the four reactions (2.1)–(2.4) are identical because the same chemical species are involved in each case and the nuclear spin state is assumed not to perturb the reaction rates. It is further assumed that barrier crossing during the four reactions occurs much faster than T_1 relaxation, so that the nuclear spin state does not change during the course of the reaction. This assumption is reasonable given that barrier crossing in biomolecular processes occurs on the timescale of ~1 μs,[43] while T_1 relaxation is on the order of 1 s.[23]

The net rate of change of the concentration of each of the chemical species A and BC can be obtained by considering the four rate equations that can be derived from eqn (2.1)–(2.4). Denoting the concentration of molecule A where the spin of interest is in spin-state $j \in \{\alpha, \beta\}$ as $[A_j]$ and focusing on eqn (2.1) as an example, the following pair of rate equations is obtained,

$$\frac{1}{2}\frac{d[A_\alpha]}{dt} = -k_1[A_\alpha]^2 + k_{-1}[B_\alpha C_\alpha] \tag{3.1}$$

$$\frac{d[B_\alpha C_\alpha]}{dt} = k_1[A_\alpha]^2 - k_{-1}[B_\alpha C_\alpha]. \tag{3.2}$$

Considering eqn (2.2)–(2.4) in a similar manner and combining all rates for $[A_\alpha]$ and $[A_\beta]$ we arrive at the following

$$\frac{d[A_i]}{dt} = -2k_1[A_i]^2 + 2k_{-1}[B_iC_i] - 2k_1[A_i][A_j] + k_{-1}[B_iC_j] + k_{-1}[B_jC_i]$$
$$i,j \in \{\alpha,\beta\},\ i \neq j \tag{4}$$

from which it can be shown that

$$\frac{d([A_\alpha] - [A_\beta])}{dt} = -2k_1\left([A_\alpha]^2 - [A_\beta]^2\right) + 2k_{-1}([B_\alpha C_\alpha] - [B_\beta C_\beta]). \tag{5}$$

Noting further that the Z-magnetization for a given probe is proportional to differences in concentrations of molecules with spin up and spin down,

$$M_Z^A = c([A_\alpha] - [A_\beta]) \tag{6.1}$$

$$M_Z^B = c([B_\alpha C_\alpha] + [B_\alpha C_\beta] - [B_\beta C_\alpha] - [B_\beta C_\beta]) \tag{6.2}$$

$$M_Z^C = c([B_\alpha C_\alpha] - [B_\alpha C_\beta] + [B_\beta C_\alpha] - [B_\beta C_\beta]) \tag{6.3}$$

where c is a constant of proportionality, allows recasting the kinetic equations that relate concentrations (for example eqn (4)) into a set of equations describing the evolution of magnetization. Starting from eqn (5) and (6) it follows directly that

$$\frac{dM_Z^A}{dt} = -2k_1[A]M_Z^A + k_{-1}(M_Z^B + M_Z^C) \tag{7}$$

where we have made use of the fact that $[A] = [A_\alpha] + [A_\beta]$ and spin relaxation has been neglected. It is noteworthy that the quadratic form of eqn (5) involving concentrations of molecules reduces to an expression that is linear in all magnetization terms, that is typical of inter-molecular exchange[24] (see below). The corresponding equation for M_Z^B is derived starting from eqn (6.2),

$$\frac{dM_Z^B}{dt} = c\left(\frac{d[B_\alpha C_\alpha]}{dt} + \frac{d[B_\alpha C_\beta]}{dt} - \frac{d[B_\beta C_\alpha]}{dt} - \frac{d[B_\beta C_\beta]}{dt}\right) \tag{8}$$

with each of the rates on the right hand side evaluated according to the reactions listed in eqn (2) above. For example, $\frac{d[B_\alpha C_\alpha]}{dt}$ that pertains to the reaction scheme in eqn (2.1) is given by eqn (3.2), with the corresponding rates for $\frac{d[B_\alpha C_\beta]}{dt}$, $\frac{d[B_\beta C_\alpha]}{dt}$, $\frac{d[B_\beta C_\beta]}{dt}$ derived from consideration of the reactions listed in eqn (2.2), (2.3) and (2.4), respectively. A straightforward calculation shows that

$$\frac{dM_Z^B}{dt} = c\left\{k_1\left([A_\alpha]^2 - [A_\beta]^2\right) - k_{-1}([B_\alpha C_\alpha] + [B_\alpha C_\beta] - [B_\beta C_\alpha] - [B_\beta C_\beta])\right\} = k_1[A]M_Z^A - k_{-1}M_Z^B. \tag{9}$$

The corresponding relation for $\frac{dM_Z^C}{dt}$ is derived identically to that for $\frac{dM_Z^B}{dt}$ or can be obtained by inspection from eqn (9) by interchanging B and C. Finally, the rate equations for Z-magnetization can be summarized succinctly as

$$\frac{d\vec{M}_Z}{dt} = \tilde{R}_L\vec{M}_Z \tag{10}$$

where

$$\tilde{R}_L = -\begin{pmatrix} 2k_1[A] + R_1^A & -k_{-1} & -k_{-1} \\ -k_1[A] & k_{-1} + R_1^B & 0 \\ -k_1[A] & 0 & k_{-1} + R_1^C \end{pmatrix}, \tag{10.1}$$

$$\vec{M}_Z = \left(M_Z^A - M_{o,A}, M_Z^B - M_{o,B}, M_Z^C - M_{o,C}\right)^+$$

In eqn (10.1) the superscript + corresponds to the transpose operator, longitudinal relaxation of a spin at each of the 3 sites

(R_1) has been added in an *ad-hoc* manner and M_o is the equilibrium longitudinal magnetization for each spin.

In the derivation of eqn (10) no assumption has been made as to whether the corresponding spins of interest in molecules B and C of the dimer are magnetically equivalent or not. In the case of magnetically equivalent spins it is possible to simplify eqn (10) by noting that $R_1^B = R_1^C$ and combining expressions for M_Z^B and M_Z^C to obtain

$$\tilde{R}_L = -\begin{pmatrix} 2k_1[A] + R_1^A & -k_{-1} \\ -2k_1[A] & k_{-1} + R_1^B \end{pmatrix} \text{ and}$$
$$\vec{M}_Z = \left(M_Z^A - M_{o,A}, M_Z^{BC} - M_{o,BC}\right)^+ \quad (10.2)$$

which is identical to the expression derived by Palmer *et al.*[24] In this limit the exchange mechanism effectively becomes two-state.

To this point we have considered only the time course for Z-magnetization due to chemical exchange. Similar equations can be derived for transverse magnetization as well. In this case it is convenient to start with eqn (2.1)–(2.4) with the modification that α, β are replaced by the eigenstates of either I_X (X-magnetization, $\alpha \rightarrow \frac{\alpha+\beta}{\sqrt{2}}$, $\beta \rightarrow \frac{\alpha-\beta}{\sqrt{2}}$) or I_Y (Y-magnetization, $\alpha \rightarrow \frac{\alpha+i\beta}{\sqrt{2}}$, $\beta \rightarrow \frac{\alpha-i\beta}{\sqrt{2}}$ where $i = \sqrt{-1}$). The effects of these changes are cosmetic in terms of the resulting expressions for the time evolution of X- or Y-magnetization due to chemical exchange. However, evolution from chemical shift then follows naturally since

$$\begin{aligned} M_X^A &= c\left(\left[A_{(\alpha+\beta)/\sqrt{2}}\right] - \left[A_{(\alpha-\beta)/\sqrt{2}}\right]\right) \\ &= \frac{c}{V}\left(N_{(\alpha+\beta)/\sqrt{2}} - N_{(\alpha-\beta)/\sqrt{2}}\right) \\ &= \frac{cN}{V}\left(P_{(\alpha+\beta)/\sqrt{2}} - P_{(\alpha-\beta)/\sqrt{2}}\right) \\ &= \frac{\gamma_A \hbar N}{2}\left(P_{(\alpha+\beta)/\sqrt{2}} - P_{(\alpha-\beta)/\sqrt{2}}\right) \end{aligned} \quad (11)$$

where $[A] = \frac{N}{V}$ with N the number of molecules in a solution of volume V, P_j is the probability of the system in state j, γ_A is the gyromagnetic ratio of spin A and $\hbar$ is Planck's constant divided by 2π. Assuming that the wavefunction for the spin in question is written generally as,

$$\psi = C_1\frac{\alpha+\beta}{\sqrt{2}} + C_2\frac{\alpha-\beta}{\sqrt{2}} \quad (12)$$

it follows that $P_{(\alpha+\beta)/\sqrt{2}} = C_1C_1^*$ and $P_{(\alpha-\beta)/\sqrt{2}} = C_2C_2^*$ where superscript star denotes complex conjugate. It can be shown that

$$\begin{aligned} \frac{d(C_1C_1^* - C_2C_2^*)}{dt} &= i\omega(C_1C_2^* - C_1^*C_2) \\ \frac{d(C_1C_2^* - C_1^*C_2)}{dt} &= i\omega(C_1C_1^* - C_2^*C_2) \end{aligned} \quad (13)$$

where ω is the Larmor frequency. Taking the derivative of both sides of eqn (11) and using eqn (13) and the relation for the expectation value of I_Y (eqn (14) below)

$$\begin{aligned} \langle\psi|I_X|\psi\rangle &= \frac{1}{2}(C_1C_1^* - C_2C_2^*) \\ \langle\psi|I_Y|\psi\rangle &= \frac{-i}{2}(C_1C_2^* - C_1^*C_2) \end{aligned} \quad (14)$$

it follows that

$$\frac{dM_X^A}{dt} = -\omega M_Y^A. \quad (15)$$

The corresponding equation for the time evolution of M_Y^A can be derived in a similar manner so that the requisite equations for the evolution of transverse magnetization become

$$\frac{d\vec{M}_+}{dt} = \tilde{R}_T\vec{M}_+ \quad (16)$$

$$\tilde{R}_T = -\begin{pmatrix} 2k_1[A] - i\omega_A + R_2^A & -k_{-1} & -k_{-1} \\ -k_1[A] & k_{-1} - i\omega_B + R_2^B & 0 \\ -k_1[A] & 0 & k_{-1} - i\omega_C + R_2^C \end{pmatrix},$$
$$\vec{M}_+ = \left(M_+^A, M_+^B, M_+^C\right)^+$$

and $M_+ = M_X + iM_Y$. In the case of magnetic equivalence of spins in molecules B and C of the dimer ($\omega_B = \omega_C$, $R_2^B = R_2^C$), eqn (16) reduces to previous expressions in the literature,[24] with

$$\tilde{R}_T = -\begin{pmatrix} 2k_1[A] - i\omega_A + R_2^A & -k_{-1} \\ -2k_1[A] & k_{-1} - i\omega_B + R_2^B \end{pmatrix},$$
$$\vec{M}_+ = \left(M_+^A, M_+^{B+C}\right)^+. \quad (17)$$

Another limiting case of interest (see below) is one where the spin probe changes environment upon dimerization in only one of the two monomers of the dimer (say B), as illustrated in Fig. 1 for formation of the asymmetric dimer. In this case it is reasonable to assume that $\omega_A = \omega_C$. Neglecting differences in transverse relaxation for the spin in A, B or C and assuming that the population of the dimer is much less than that of the monomer eqn (16) reduces to

$$\tilde{R}_T = -\begin{pmatrix} k_1[A] - i\omega_A + R_2 & -k_{-1} \\ -k_1[A] & k_{-1} - i\omega_B + R_2 \end{pmatrix},$$
$$\vec{M}_+ = \left(M_+^A, M_+^B\right)^+ \quad (18)$$

and the exchange is effectively two-state, as in the case of a symmetric dimerization process (eqn (17)), although the rate matrices are different in each case. The factor of 2 difference in the $k_1[A]$ terms for the two cases reflects the fact that in the exchange event leading to the production of the symmetric dimer two molecules of monomer (A) are lost, while for the asymmetric dimer and in the limit where eqn (18) applies only a single molecule of A is lost upon formation of the dimer since one molecule of the dimer remains 'A like'.

In the case of exchange leading to a symmetric dimer or for the case where an asymmetric dimer is formed under the conditions considered above eqn (17) and (18), establish

that the resulting dispersion data will be well fit to a model of two-site exchange $S_1 \underset{k'_{-1}}{\overset{k'_1}{\rightleftharpoons}} S_2$

$$\tilde{R}_T = -\begin{pmatrix} k_1' - i\omega_1 + R_2 & -k_{-1}' \\ -k_1' & k_{-1}' - i\omega_2 + R_2 \end{pmatrix} \quad (19)$$

from which $k_{ex} = k_1' + k_{-1}'$ and the fractional populations, p_1 and $p_2 = 1 - p_1$, of the exchanging species are obtained. Further, the forward $k_1' = p_2 k_{ex}$ and reverse $k_{-1}' = p_1 k_{ex}$ rates can be readily calculated from extracted values of k_{ex} and the populations.

Of course, although the data are well fit by a two-site exchange model the interpretation of the resulting fitted parameters still depends critically on the actual exchange process. For the symmetric dimer case considered above a comparison of eqn (17) and (19), shows that

$$k_{ex} = 2k_1[A] + k_{-1} \quad (20)$$

with $k_{-1}' = p_1 k_{ex} = k_{-1}$, $k_1' = p_2 k_{ex} = 2k_1[A]$ and

$$p_1 = \frac{[A]}{[A] + 2[BC]}. \quad (21)$$

In contrast, when an asymmetric dimer is formed the equations become

$$k_{ex} = k_1[A] + k_{-1} \quad (22)$$

with $k_{-1}' = p_1 k_{ex} = k_{-1}$, $k_1' = p_2 k_{ex} = k_1[A]$ and

$$p_1 = \frac{[A]}{[A] + [BC]}. \quad (23)$$

Thus, while the same value for k_{-1} is obtained *via* both models the extracted on-rates and populations are model dependent.

Numerical simulations of CPMG profiles for symmetric and asymmetric dimerization

In the section above we have derived a set of coupled differential equations that describe the evolution of magnetization due to the exchange reaction $2A \underset{k_{-1}}{\overset{k_1}{\rightleftharpoons}} BC$ and discussed limiting conditions where the resulting 3×3 exchange matrix reduces to a simple 2×2 form that is indistinguishable from what is obtained using a model of two-site chemical exchange. In order to test these limiting conditions and to establish when they break down we have simulated CPMG profiles for various input parameters for a system undergoing exchange using eqn (16) and fit the resulting profiles using the 2-state model of eqn (19). In an initial set of computations the transverse relaxation rates (R_2) for the monomer and dimer were set to 10 and 15 s^{-1}, respectively, consistent with experimental observations for apoSOD1^{2SH}.[41] Exchange rates k_1 and k_{-1} were assumed to be 30 000 M^{-1} s^{-1} and 705 s^{-1}, respectively, corresponding to a K_D of 23.5 mM, and a total protein concentration of 1.5 mM was used. The chosen K_D, together with the protein concentration, ensures approximately 5–10% of the excited dimeric state, which is ideal for CPMG experiments. As we discuss below, the values of k_1 and k_{-1} were selected to yield k_{ex} values on the order of 800 s^{-1} (the exact number depends on whether the dimerization process is symmetric or asymmetric), that is well within the sensitive region of the CPMG experiment. CPMG profiles were simulated for 12 ^{15}N chemical shift differences ($\Delta\varpi$) ranging from 1.4–7.4 ppm at two B_0 field strengths of 11.8 T (500 MHz ^1H frequency) and 18.8 T (800 MHz ^1H frequency). Noise was not added to the simulated data so that poor fits that result from using an incorrect model of exchange can be distinguished from deviations resulting from the added noise, although errors corresponding to 2% of each $R_{2,eff}$ value were included. The resulting dispersion profiles were then fit as a group and extracted parameters compared with the input values.

In the case of exchange involving a symmetric dimer the underlying equations are exactly 2-state and we would expect to get very similar fitted parameters based on eqn (19) as those input into eqn (16) with $\varpi_B = \varpi_C$. Based on the input values listed above, expected k_{ex} and p_2 values are 786 s^{-1} and 10.3% (eqn (20) and (21)). Extracted values for k_{ex}(766 ± 6 s^{-1}) and p_2(10.08 ± 0.05%) obtained by fitting dispersion curves to eqn (19) (that assumes that the intrinsic relaxation rates of monomer and dimer are the same) are in good agreement with input parameters as are the fitted $\Delta\varpi$ values (Fig. 2A and B).

Next we examined the case of asymmetric dimer formation with $\varpi_A = \varpi_C$, corresponding to the situation where the chemical shift of the probe spin differs in only one of the two protomers of the dimeric complex from that in the monomer. Expected values of k_{ex} and p_2 are 744 s^{-1} and 5.2% that agree well with fitted parameters of k_{ex}(726 ± 8 s^{-1}) and p_2(5.03 ± 0.04%). Fitted and input $\Delta\varpi$ values are in excellent agreement as well (Fig. 2C and D). Taken together, this supports the use of the two-state approximation for the three-state asymmetric dimer model (eqn (18)) in the limit where the population of the dimeric state is small compared to that of the monomer.

Finally, we considered the asymmetric dimerization model in the case where $\varpi_B \neq \varpi_C$ and simulated dispersion profiles using the same parameters as above. Here the same set of ϖ_C values was used as for ϖ_B, except that for each residue with a given ϖ_B a random (and different) ϖ_C from the set was chosen. As expected, the simulated CPMG profiles cannot be adequately fit to a two-state exchange model (Fig. 2E and F) and the k_{ex}(832 ± 7 s^{-1}), p_2(8.13 ± 0.04%) and $\Delta\varpi$ values extracted from the fit do not agree with the expected values, demonstrating that in the general case, asymmetric dimerization is not a two-state process.

Having confirmed *via* simulation that three-site exchange asymmetric dimerization effectively reduces to a two-site exchange process in the limiting case where $\varpi_A = \varpi_C$ and the excited (dimeric) state is only sparsely populated, $p_B = p_C \ll p_A$, we next explored in more detail the exchange conditions for which the two-state approximation is reasonable, assuming throughout that $\varpi_A = \varpi_C$. First, we systematically varied both k_1 and k_{-1} values such that the input k_{ex} (eqn (22)) used in simulations ranged from ~200 to ~2000 s^{-1}, which is typically the regime over which CPMG experiments are sensitive. For all simulations $K_D = \frac{k_{-1}}{k_1}$ was kept constant at 9 mM, the overall

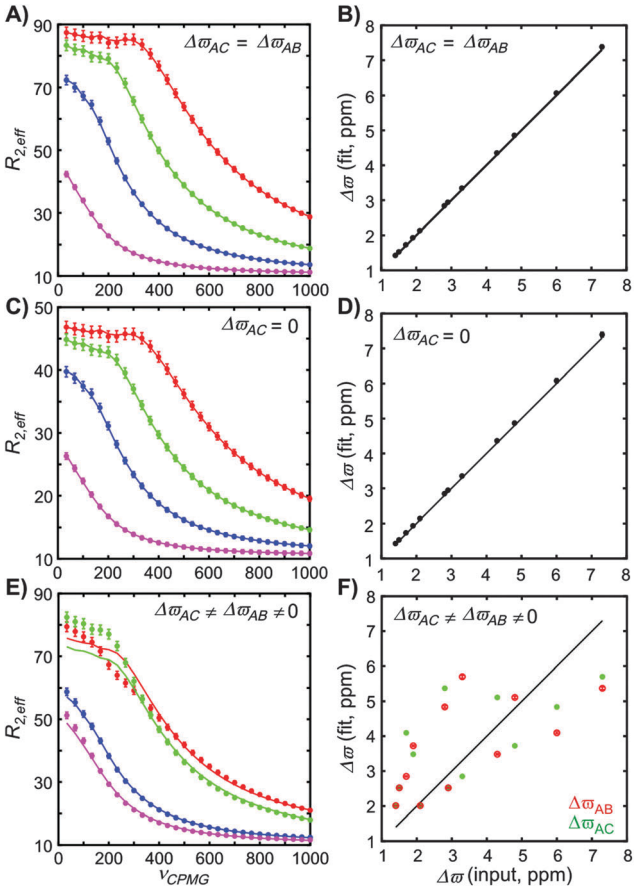

Fig. 2 Representative ^{15}N CPMG dispersion data simulated using eqn (16) for (A) symmetric dimerization ($\varpi_B = \varpi_C$), (C) asymmetric dimerization with $\varpi_A = \varpi_C$ and (E) asymmetric dimerization with $\varpi_B \neq \varpi_C$. Colors distinguish between different $\Delta\varpi_{AB}$ values chosen in the simulations (red: 7.3 ppm, green: 4.8 ppm, blue: 2.9 ppm and magenta: 1.4 ppm). Solid lines are global fits of the data to a two-state exchange model, as described in the text. Values of $R_{2,eff}$ and ν_{CPMG} are effective transverse relaxation rates and the rate of application of refocusing pulses, respectively.[24] (B, D and F) Linear correlation plots of chemical shift differences between the ground and excited states extracted from fits of simulated CPMG data (*Y*-axis) *vs.* input values (*X*-axis). Solid lines are $y = x$. In panel F, the $\Delta\varpi$ values from the fit are compared to both input $\Delta\varpi_{AB}$ (red) and $\Delta\varpi_{AC}$ (green) values.

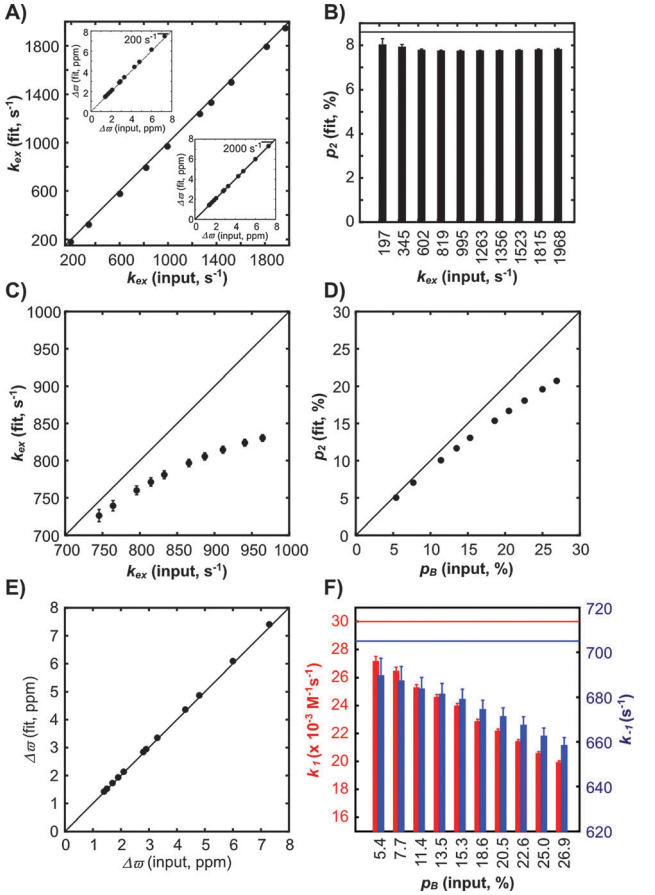

Fig. 3 Comparison between input and extracted exchange parameters from fits of CPMG data simulated for asymmetric dimer formation with $\varpi_A = \varpi_C$ (eqn (16)). A model of two-site chemical exchange (eqn (19)) was used to fit the simulated data, as described in the text. (A) Linear correlation plot of k_{ex} values extracted from fitting simulated ^{15}N CPMG dispersion curves ($\varpi_A = \varpi_C$, and $p_B = p_C = 8.6\%$, $K_D = 9$ mM) with input values. The insets show correlation plots between input and fitted $\Delta\varpi$ values for k_{ex} values of 200 s^{-1} and 2000 s^{-1}. (B) p_2 values obtained from fits of simulated ^{15}N dispersion profiles as a function of each input k_{ex} value indicated along the *X*-axis. The horizontal line denotes the expected value of p_2 (8.6%). (C, D and F) Extracted exchange parameters as in (A and B) from fits of simulated dispersion profiles (k_1 = 30 000 M^{-1} s^{-1} and k_{-1} = 705 s^{-1}) obtained by changing the overall protein concentration. The chemical shift correlation plot for this set of simulations at the highest protein concentration of 15 mM ($p_B = 26.9\%$) is shown in panel E. (F) k_1 and k_{-1} values derived from fits as a function of input p_B values. Horizontal bars indicate the input rates.

protein concentration was 1 mM, $p_B = p_C = 8.6\%$, monomer and dimer R_2 values were set to 10 and 15 s^{-1}, respectively, and dispersion profiles simulated for 12 $\Delta\varpi$ values ranging from 1.4 to 7.4 ppm, as above. The resulting CPMG profiles, generated with eqn (16), were then fit to a two-site exchange model (eqn (19)) to extract k_{ex}, p_2 and $\Delta\varpi$. All three parameters correlate well with the expected values (Fig. 3A and B), establishing that the two-state approximation is valid over the entire range of exchange rates probed by CPMG experiments, so long as p_2 is small.

Subsequently, $p_B = p_C$ values were systematically varied from ~5 to ~30% by changing the total protein concentration, keeping k_1 (30 000 s^{-1}) and k_{-1}(705 s^{-1}) constant; note that k_{ex} values range from ~750 s^{-1} to ~950 s^{-1} as a result of the change in the concentration of free protein. All other parameters were identical to those used in the simulations above. The resultant CPMG profiles generated using eqn (16) were fit with eqn (19), and the parameters obtained plotted in Fig. 3C–F. Notably, the input and fitted exchange parameters diverge as p_B increases (Fig. 3C, D and F), since the two-state approximation breaks down for dimer populations greater than approximately 15%. Interestingly, the fitted $\Delta\varpi$ values are correct over the complete range of p_B values used in the simulations, with the correlation between fitted and input chemical shift differences illustrated for the maximum p_B value (27%) in Fig. 3E.

An application to conformational exchange in apoSOD1^{2SH}

In a recent study[41] we have probed the energy landscape of apoSOD1^{2SH}, an immature form of SOD1 that is monomeric,

metal free and lacking the stabilizing disulfide bond between conserved cysteines at positions 57 and 146.[44] Using a combination of both CPMG and CEST experiments we showed that apoSOD1^{2SH} is highly dynamic and that it interconverts between four different conformational states on the millisecond timescale. Two of the states have features that are native-like. One of the exchange processes leads to a native dimer structure, while the second results in the formation of a key helix that helps stabilize the Zn-bound form of the mature enzyme. The second pair of exchange events results in the formation of aberrant oligomers whose structures have been modeled using chemical shift restraints and the program HADDOCK,[42] producing symmetric and asymmetric dimers as shown in Fig. 1. Here CPMG relaxation dispersion experiments were particularly useful because the relatively small chemical shift differences of both ^{15}N and methyl-^{13}C probes in the interconverting states made it difficult to resolve minor state dips in CEST experiments.

Fig. 4 shows ^{15}N relaxation dispersion profiles as a function of total protein concentration for a number of sites in apoSOD1^{2SH}

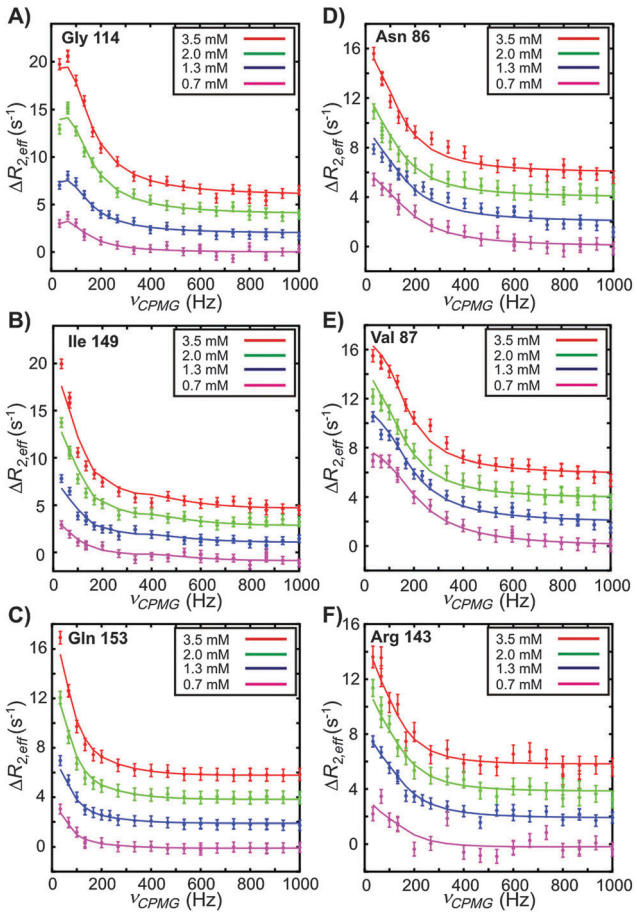

Fig. 4 Representative ^{15}N CPMG relaxation dispersion profiles recorded on samples of apoSOD1^{2SH} (600 MHz ^{1}H frequency, 25 °C) as a function of concentration from 0.7 mM to 3.5 mM for residues reporting on symmetric (A–C) and asymmetric dimerization (D–F). The y-axis is $\Delta R_{2,\mathrm{eff}} = R_{2,\mathrm{eff}} - R_{2,\infty} + c$, where $R_{2,\infty}$ is the value of $R_{2,\mathrm{eff}}(\nu_{\mathrm{CPMG}} = \infty)$ and c is a constant offset applied for clarity (c = 0 s^{-1} (0.7 mM), c = 2 s^{-1} (1.3 mM), c = 4 s^{-1} (2.0 mM) and c = 6 s^{-1} (3.5 mM)). Solid lines are global fits of the data at each concentration to a two-state exchange model.

that report on the symmetric (A–C) and asymmetric (D–F) dimerization processes. As expected for an oligomerization event where the monomer is the dominant form in the solution, dispersion profiles become larger with protein concentration because the population of the dimer increases. Shown also are best fits of the dispersion curves (circles) to a model of two-site chemical exchange (solid lines). Consistent with expectations for a symmetric dimerization process, the profiles are very well fit to a two-site exchange mechanism with a reduced chi-squared (χ_{red}^2) of 0.7–1.2 (see discussion above). Notably, fits of profiles from residues reporting on the asymmetric process are essentially equally good (χ_{red}^2 = 1.0–1.5). This is expected when (i) the relaxation rates of the spin in question are similar in both the monomer and the dimer, (ii) the chemical shift of the spin in one of monomers of the dimer is identical to that in the free monomer and (iii) the dimer population is low (eqn (18)). Our previous studies of apoSOD1^{2SH} have established that both symmetric and asymmetric dimers are populated to approximately 2–3% that of the dominant monomer in solution (25 °C).[41] Further, structural models for the asymmetric dimer clearly show that while one set of nuclei reporting on the exchange event locate to the dimer interface, the corresponding spins from the second monomer are well removed from the interface so as not to be influenced by the exchange process (Fig. 1). Finally, while R_2 values for the monomer and dimer species are not expected to be the same, simulations establish that the approximate 1.5-fold increase in average R_2 rates from monomer to dimer[41] does not significantly influence the quality of the fits of the CPMG data to a two-site exchange model, as seen above.

The simulated CPMG data presented in Fig. 2 along with the experimental data of Fig. 4 make the point that obtaining high quality two state fits of dispersion profiles does not prove that the underlying exchange mechanism is a simple interconversion between a pair of conformers. Indeed, even for a dimerization process, distinguishing between symmetric and asymmetric association is difficult in cases where the magnetic environment of the probe spin(s) is similar in the monomer and one (but not the other) of the molecules of the dimer. Such a distinction may only be possible by analysis of the resulting dimeric structures that are produced, for example, with chemical shift restraints and a molecular docking program such as HADDOCK,[42] as was done for apoSOD1^{2SH}.[41]

Fig. 5 plots $1/p_2$ as a function of the concentration of free apoSOD1^{2SH}, for both symmetric and asymmetric dimerization processes. Values of p_2 were obtained from fits of the concentration dependent CPMG dispersion data assuming a two-site model of exchange (eqn (19)) and are related to K_{D} in a straightforward manner,

$$\frac{1}{p_2} = 1 + \frac{K_{\mathrm{D}}}{\alpha[\mathrm{A}]} \qquad (24)$$

where α = 1 or 2 for asymmetric or symmetric processes, respectively. Values of (K_{D}, k_{-1}, k_1) = (73 ± 7 mM, 154 ± 40 s^{-1}, 2110 ± 600 M^{-1} s^{-1}; symmetric) and (67 ± 7 mM, 570 ± 130 s^{-1}, 8475 ± 2130 M^{-1} s^{-1}; asymmetric) are obtained,

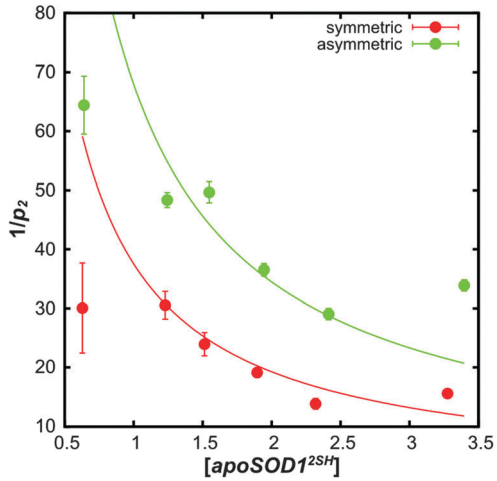

Fig. 5 Variation in the extracted excited state population (p_2) from fits of experimental CPMG dispersion data (Fig. 4) as a function of free protein (apoSOD1^{2SH}) concentration for symmetric (red) and asymmetric (green) dimerization processes. Solid lines are fits of the data to eqn (24) of the text. An outlier in both curves is noted for the data point recorded at the lowest concentration. The origin of the problem is unclear, however it is worth noting that this point is less reliable than the others because it is derived from NMR spectra with the lowest signal-to-noise ratio and the smallest dispersions profiles and CPMG data were acquired at only a single B_0 field in this case.

where k_{-1} is calculated as the average of $(1 - p_2) \times k_{ex}$ over all 6 different protein concentrations and k_1 is obtained from the relation $k_1 = \frac{k_{-1}}{K_D}$. Although the apoSOD1^{2SH} non-native dimers that are probed by CPMG relaxation dispersion studies are formed only very weakly and would not normally accumulate *in vivo*, it may be that association is enhanced in the crowded cellular environment. Further, it may be possible to increase the concentration of apoSOD1^{2SH} under conditions of oxidative stress or through the introduction of mutations, leading to larger populations of aberrant oligomers. These could then serve as templates for assembly of high molecular weight species by recruitment of other native and non-native monomer and dimer molecules, as has been suggested by *in vitro*[45,46] and *in vivo*[47] experiments on SOD1 misfolding and fibrillation. Notably, this work highlights the fact that it is possible to study association processes that are extremely weak using NMR relaxation methods, a powerful and rather unique feature of this technology.

Concluding remarks

We have presented a set of equations for the time dependence of magnetization due to the exchange reaction $2A \underset{k_{-1}}{\overset{k_1}{\rightleftharpoons}} BC$ whereby a pair of monomers associate to form a homodimer. Different expressions are derived for the cases of symmetric and asymmetric dimer formation. Central to the description has been the development of a spin-state selective formalism whereby exchange for a spin 1/2 particle is described by separate sets of equations for spins in α and β spin-states. This approach clarifies why non-linear equations describing rates of change of concentrations of molecules reduce to linear expressions for magnetization exchange (eqn (4)–(7)). Effectively, the dimerization reaction considered here can be thought of as an exchange event occurring between a small number of NMR active nuclei whose population is given by Boltzmann's law (M_Z^A, in eqn (9)) and a bulk population of non-NMR active nuclei ([A] in eqn (9)). The sets of derived equations have been used in the analysis of a pair of exchange events involving the interconversion of monomeric apoSOD1^{2SH} to symmetric and asymmetric homodimers. With the continued development of sensitive NMR experiments for probing exchange it has become possible to study an expanding number of different conformational changes in proteins. Equally important is the development of the appropriate models to analyze the exchange kinetics so that the extracted parameters reflect the physical exchange process studied.

Materials and methods

ApoSOD1^{2SH} was overexpressed and purified and CPMG experiments recorded and analyzed as reported previously.[41] Briefly, ^{15}N CPMG relaxation dispersion experiments were recorded on U-^{15}N or U-[^{15}N,^{13}C] samples of apoSOD1^{2SH} ranging in concentration from 0.7–3.5 mM using a previously reported constant-time pulse sequence.[48] Data was recorded at 2 B_0 field strengths (600 MHz and 800 MHz ^{1}H Larmor frequency) for all sample concentrations except at 0.7 mM for which CPMG profiles were acquired only at 600 MHz. A constant-time CPMG exchange element (T_{CPMG}) of 30 ms was used for all datasets and approximately 20 CPMG frequencies ranging from 33.3 to 1000 Hz were employed, with 3–5 frequencies repeated for error analysis. Peak intensities were extracted using FuDA (http://pound.med.utoronto.ca/software.html) and converted to effective transverse relaxation rates $R_{2,eff}$ using the equation $R_{2,eff} = (1/T_{CPMG}) \ln(I_0/I)$. CPMG dispersion profiles were fit to a two-state model of chemical exchange by propagating the relevant Bloch–McConnell equations using the software package CATIA (http://pound.med.utoronto.ca/software.html). Errors in the fit parameters were estimated using the covariance matrix method.[49]

Acknowledgements

This work was supported by grants from the CIHR (E.M.M. and L.E.K.) and NSERC (L.E.K.). L.E.K. holds a Canada Research Chair in Biochemistry. This paper is dedicated to Prof. Bill Reynolds, University of Toronto, in honor of 50 years of doing NMR.

References

1 M. Karplus and J. Kuriyan, *Proc. Natl. Acad. Sci. U. S. A.*, 2005, **102**, 6679–6685.
2 R. Ishima and D. A. Torchia, *Nat. Struct. Mol. Biol.*, 2000, **7**, 740–743.
3 D. D. Boehr, D. McElheny, H. J. Dyson and P. E. Wright, *Science*, 2006, **313**, 1638–1642.

4 K. Vamvaca, B. Vögeli, P. Kast, K. Pervushin and D. Hilvert, *Proc. Natl. Acad. Sci. U. S. A.*, 2004, **101**, 12860–12864.
5 M. Wolf-Watz, V. Thai, K. Henzler-Wildman, G. Hadjipavlou, E. Z. Eisenmesser and D. Kern, *Nat. Struct. Mol. Biol.*, 2004, **11**, 945–949.
6 S. Rozovsky and A. E. McDermott, *J. Mol. Biol.*, 2001, **310**, 259–270.
7 J. Kim, L. R. Masterson, A. Cembran, R. Verardi, L. Shi, J. Gao, S. S. Taylor and G. Veglia, *Proc. Natl. Acad. Sci. U. S. A.*, 2015, **112**, 3716–3721.
8 D. D. Boehr, R. Nussinov and P. E. Wright, *Nat. Chem. Biol.*, 2009, **5**, 789–796.
9 P. Csermely, R. Palotai and R. Nussinov, *Trends Biochem. Sci.*, 2010, **35**, 539–546.
10 S.-R. Tzeng and C. G. Kalodimos, *Curr. Opin. Struct. Biol.*, 2011, **21**, 62–67.
11 T. Mittag, L. E. Kay and J. D. Forman-Kay, *J. Mol. Recognit.*, 2010, **23**, 105–116.
12 F. Chiti and C. M. Dobson, *Nat. Chem. Biol.*, 2008, **5**, 15–22.
13 P. Neudecker, P. Robustelli, A. Cavalli, P. Walsh, P. Lundström, A. Zarrine-Afsar, S. Sharpe, M. Vendruscolo and L. E. Kay, *Science*, 2012, **336**, 362–366.
14 P. Hammarström, R. L. Wiseman, E. T. Powers and J. W. Kelly, *Science*, 2003, **299**, 713–716.
15 A. Quintas, D. C. Vaz, I. Cardoso, M. J. M. Saraiva and R. M. Brito, *J. Biol. Chem.*, 2001, **276**, 27207–27213.
16 Z. Lai, W. Colón and J. W. Kelly, *Biochemistry*, 1996, **35**, 6470–6482.
17 D. Canet, A. M. Last, P. Tito, M. Sunde, A. Spencer, D. B. Archer, C. Redfield, C. V. Robinson and C. M. Dobson, *Nat. Struct. Mol. Biol.*, 2002, **9**, 308–315.
18 A. Galaleldeen and P. J. Hart, *Protein Misfolding, Aggregation, and Conformational Diseases*, Springer, 2007, pp. 327–344.
19 J. S. Valentine and P. J. Hart, *Proc. Natl. Acad. Sci. U. S. A.*, 2003, **100**, 3617–3622.
20 P. Stathopulos, J. Rumfeldt, G. Scholz, R. Irani, H. Frey, R. Hallewell, J. Lepock and E. Meiering, *Proc. Natl. Acad. Sci. U. S. A.*, 2003, **100**, 7021–7026.
21 H. R. Broom, J. A. Rumfeldt and E. M. Meiering, *Essays Biochem.*, 2014, **56**, 149–165.
22 T. R. Jahn, M. J. Parker, S. W. Homans and S. E. Radford, *Nat. Struct. Mol. Biol.*, 2006, **13**, 195–201.
23 J. Cavanagh, W. J. Fairbrother, A. G. Palmer and N. J. Skelton, *Protein NMR spectroscopy: Principles and Practice*, Academic Press, 1995.
24 A. G. Palmer, C. D. Kroenke and J. P. Loria, *Methods Enzymol.*, 2000, **339**, 204–238.
25 N. L. Fawzi, J. Ying, R. Ghirlando, D. A. Torchia and G. M. Clore, *Nature*, 2011, **480**, 268–272.
26 A. Sekhar and L. E. Kay, *Proc. Natl. Acad. Sci. U. S. A.*, 2013, **110**, 12867–12874.
27 A. Mittermaier and L. E. Kay, *Science*, 2006, **312**, 224–228.
28 H. Y. Carr and E. M. Purcell, *Phys. Rev.*, 1954, **94**, 630.
29 S. Meiboom and D. Gill, *Rev. Sci. Instrum.*, 1958, **29**, 688–691.
30 S. Forsén and R. A. Hoffman, *J. Chem. Phys.*, 1963, **39**, 2892–2901.
31 E. N. Nikolova, E. Kim, A. A. Wise, P. J. O'Brien, I. Andricioaei and H. M. Al-Hashimi, *Nature*, 2011, **470**, 498–502.
32 F. A. Mulder, N. R. Skrynnikov, B. Hon, F. W. Dahlquist and L. E. Kay, *J. Am. Chem. Soc.*, 2001, **123**, 967–975.
33 P. Vallurupalli, G. Bouvignies and L. E. Kay, *J. Am. Chem. Soc.*, 2012, **134**, 8148–8161.
34 J. S. Valentine, P. A. Doucette and S. Zittin Potter, *Annu. Rev. Biochem.*, 2005, **74**, 563–593.
35 P. Zetterström, K. S. Graffmo, P. M. Andersen, T. Brännström and S. L. Marklund, *NeuroMol. Med.*, 2013, **15**, 147–158.
36 S. Matsumoto, H. Kusaka, H. Ito, N. Shibata, T. Asayama and T. Imai, *Clin. Neuropathol.*, 1995, **15**, 41–46.
37 M. S. Rotunno and D. A. Bosco, *Front. Cell. Neurosci.*, 2013, **7**, 1–16.
38 P. B. Stathopulos, J. A. Rumfeldt, F. Karbassi, C. A. Siddall, J. R. Lepock and E. M. Meiering, *J. Biol. Chem.*, 2006, **281**, 6184–6193.
39 Y. Sheng, M. Chattopadhyay, J. Whitelegge and J. Selverstone Valentine, *Curr. Top. Med. Chem.*, 2012, **12**, 2560–2572.
40 Y. Furukawa and T. V. O'Halloran, *J. Biol. Chem.*, 2005, **280**, 17266–17274.
41 A. Sekhar, J. Rumfeldt, H. R. Broom, C. M. Doyle, G. Bouvignies, E. M. Meiering and L. E. Kay, *eLife*, 2015, **4**, e07296.
42 C. Dominguez, R. Boelens and A. M. Bonvin, *J. Am. Chem. Soc.*, 2003, **125**, 1731–1737.
43 H. S. Chung and W. A. Eaton, *Nature*, 2013, **502**, 685–688.
44 E. D. Getzoff, D. E. Cabelli, C. L. Fisher, H. E. Parge, M. S. Viezzoli, L. Banci and R. A. Hallewell, *Nature*, 1992, **358**, 347–351.
45 M. Chattopadhyay, A. Durazo, S. H. Sohn, C. D. Strong, E. B. Gralla, J. P. Whitelegge and J. S. Valentine, *Proc. Natl. Acad. Sci. U. S. A.*, 2008, **105**, 18663–18668.
46 K. A. Vassall, H. R. Stubbs, H. A. Primmer, M. S. Tong, S. M. Sullivan, R. Sobering, S. Srinivasan, L.-A. K. Briere, S. D. Dunn and W. Colón, *Proc. Natl. Acad. Sci. U. S. A.*, 2011, **108**, 2210–2215.
47 L. I. Grad, W. C. Guest, A. Yanai, E. Pokrishevsky, M. A. O'Neill, E. Gibbs, V. Semenchenko, M. Yousefi, D. S. Wishart and S. S. Plotkin, *Proc. Natl. Acad. Sci. U. S. A.*, 2011, **108**, 16398–16403.
48 P. Vallurupalli, D. F. Hansen, E. Stollar, E. Meirovitch and L. E. Kay, *Proc. Natl. Acad. Sci. U. S. A.*, 2007, **104**, 18473–18477.
49 J. Taylor, *Introduction to Error Analysis: The Study of Uncertainties in Physical Measurements*, University Science Books, 1997.

